Structural Engineering and Mechanics, Vol. 22, No. 3 (2006) 351-370
DOI: http://dx.doi.org/10.12989/sem.2006.22.3.351

Seismic analysis of arch dams including dam-reservoir interaction via a continuum damage model

M. Karaton† and Y. Calayır

Firat University, Department of Civil Engineering, Elazig, Turkey

A. Bayraktar

Karadeniz Technical University, Department of Civil Engineering, Trabzon, Turkey

(Received December 10, 2004, Accepted November 2, 2005)

Abstract. In this study, the earthquake damage response of the concrete arch dams was investigated including dam-reservoir interaction. A continuum damage model which is a second-order tensor and includes the strain softening behavior was selected for the concrete material. Fluid-structure interaction problem was modeled by Lagrangian approach. Sommerfeld radiation condition was applied to the truncated boundary of reservoir. The improved form of the HHT-α time integration algorithm was used in the solution of the equations of motion. The arch dam Type 5 was selected for numerical application. For the dynamic input, acceleration records of the 10 December 1967 Koyna earthquake were chosen. These records were scaled with earthquake acceleration scale factor (EASF) and then used in the analyses. Solutions were obtained for empty and full reservoir cases. The effects of EASF and damping ratio on the response of the dam were studied.

Key words: damage model; dam-reservoir interaction; seismic response; arch dam.

1. Introduction

Concrete arch dams are expected to retain the water impounded in the reservoir during a safety evaluation earthquake. Although damage to the concrete in the form of limited cracking is acceptable, cracking can not be extensive enough to cause instability of the dam structure and loss of the reservoir. Therefore, reliable analytical procedures to evaluate the earthquake response of arch dams are necessary to design earthquake resistant dams and to evaluate the earthquake safety of existing dams.

Concrete dams are constructed or designed to resist two levels of earthquakes: Design Base Earthquake (DBE) as well as Maximum Credible Earthquake (MCE). The dam response generally remains in the elastic range for the first level while cracking and structural damage are expected for the second one (NCR 1990, Ghrib and Tinawi 1995). However, MCE is an extremely rare event capable of producing the largest ground motion that could ever occur at the dam site. A linear

† Corresponding author, E-mail: mkaraton@firat.edu.tr

earthquake analysis of an arch dam subjected to strong ground motion generally gives peak tensile stresses greater than the dynamic tensile strength of concrete. Consequently, damage may occur in the dam due to these stresses. Non-linear procedures are therefore required to assess the seismic safety of concrete dams in earthquake-prone areas. These procedures generally involve either finite or boundary element mathematical models (Batta and Pekau 1989, Ghrib and Tinawi 1995).

In finite element calculations of concrete structures, one method which is known as the discrete crack approach (DCA) uses fracture mechanics concepts to model the discrete cracking observed in concrete. One another method which is termed as smeared crack approach (SCA) utilizes continuum models. The SCA is based on changes in the constitutive laws governing the behavior of concrete. Continuum damage mechanics (CDM) which is based on the same philosophy of smeared crack approach offers a particularly interesting context where damage evolution can be simulated. Damage mechanics provides an average measure of material degradation due to micro-cracking, interfacial de-bonding, nucleation and coalescence of voids. The non-linear analysis based on CDM provides the most realistic results (Mazars and Pijaudier-Cabot 1983). Some investigators have studied the seismic response of concrete dams using CDM (Ghrib and Tinawi 1995, Lee and Fenves 1998, Valliappan *et al.* 1999, Calayır and Karaton 2005).

Reservoir-dam problem is a fluid-structure interaction problem. Fluid-structure interaction problems can be modeled by using one from Eularian, Lagrangian and Added mass approaches (Calayır *et al.* 1996). In the added-mass representation of dam-water interaction, the hydrodynamic pressures exerted on the face of the dam due to the earthquake ground motion is equivalent to the inertia forces of a body of water attached to the dam. Dam-reservoir interaction problem are generally solved by using finite element method for Eulerian and Lagrangian approaches. Reservoir and dam domains have pressure and displacement freedoms, respectively, for the Eulerian approach. However, both domains have displacement freedoms for the Lagrangian approach. Hence, the Eularian approach requires to being used special interface element for dam-reservoir interaction while it is not required in case of Lagrangian approach. The programming of the dynamic interaction problems of fluid-structure systems using the Lagrangian approach and incorporating this program into existing computer programs is simpler with respect to that of the Eulerian approach. Nevertheless, the requirement for computing memory and time are increased because the Lagrangian approach requires to be used significantly more degrees of freedom.

In this study, the earthquake damage response of the concrete arch dams was investigated including dam-reservoir interaction. A continuum damage model which is a second-order tensor and includes the strain softening behavior was selected for the concrete material. Fluid-structure interaction problem was modeled by Lagrangian approach. Sommerfeld radiation condition was applied to the truncated boundary of reservoir. The arch dam Type 5 was selected for numerical application. For the dynamic input, acceleration records of the 10 December 1967 Koyna earthquake were chosen. These records are scaled with the EASF and then used in the analyses. Solutions were obtained for empty and full reservoir cases. The effects of the EASF value and damping ratio on the response of the dam were discussed.

2. Anisotropic damage model for concrete

Distributed micro-cracks in material causes a reduction of the net area capable of supporting stresses and leads the material degradation. The loss of rigidity of the material is followed due to

defining a fictitious undamaged material related to the damaged one through a number of hypotheses. Using the fact that the internal forces acting on any damaged section are the same as the one before damage, the following relation between the Cauchy stress vector $\{\tilde{\sigma}\}$ and the effective stress (net stress) vector $\{\tilde{\sigma}^{+}\}$ can be written for 3-D case (Valliappan *et al.* 1999, Karaton 2004)

$$\{\tilde{\sigma}^{+}\} = [\Psi]\{\tilde{\sigma}\} \tag{1}$$

in which $[\Psi]$ is the damage matrix and it may be given by

$$[\Psi] = \begin{bmatrix} 1/(1-d_1) & 0 & 0 & 0 & 0 & 0 \\ 0 & 1/(1-d_2) & 0 & 0 & 0 & 0 \\ 0 & 0 & 1/(1-d_3) & 0 & 0 & 0 \\ 0 & 0 & 0 & 1/(1-d_2) & 0 & 0 \\ 0 & 0 & 0 & 1/(1-d_1) & 0 & 0 \\ 0 & 0 & 0 & 0 & 1/(1-d_1) & 0 \\ 0 & 0 & 0 & 0 & 1/(1-d_3) & 0 \\ 0 & 0 & 0 & 0 & 0 & 1/(1-d_3) \\ 0 & 0 & 0 & 0 & 0 & 1/(1-d_2) \end{bmatrix} \tag{2}$$

This matrix includes d_1, d_2 and d_3 damage parameters in the three principal stress directions and these parameters are defined as

$$d_i = \frac{A_i - A_i^{+}}{A_i} \qquad i = 1, 2, 3 \tag{3}$$

where A_i and A_i^{+} are the total and net areas. The effective stress vector is not symmetric. To restore symmetry, different approaches may be applied (Valliappan *et al.* 1999). If the symmetrized effective stress vector $\{\tilde{\sigma}^{*}\}$ is defined as

$$\{\tilde{\sigma}^{*}\}^{T} = \{\tilde{\sigma}_1^{*} \;\; \tilde{\sigma}_2^{*} \;\; \tilde{\sigma}_3^{*} \;\; \tilde{\sigma}_{12}^{*} \;\; \tilde{\sigma}_{13}^{*} \;\; \tilde{\sigma}_{23}^{*}\}$$

$$= \left\{ \tilde{\sigma}_1^{+} \;\; \tilde{\sigma}_2^{+} \;\; \tilde{\sigma}_3^{+} \sqrt{\frac{(\tilde{\sigma}_{12}^{+})^2 + (\tilde{\sigma}_{21}^{+})^2}{2}} \sqrt{\frac{(\tilde{\sigma}_{13}^{+})^2 + (\tilde{\sigma}_{31}^{+})^2}{2}} \sqrt{\frac{(\tilde{\sigma}_{23}^{+})^2 + (\tilde{\sigma}_{32}^{+})^2}{2}} \right\} \tag{4}$$

then, this vector can be related to the Cauchy stress vector by

$$\{\tilde{\sigma}^{*}\} = [\Psi^{*}(d_i)]\{\tilde{\sigma}\} \tag{5}$$

where $[\Psi^{*}]$ is the damage matrix related to $\{\tilde{\sigma}^{*}\}$. All non-diagonal terms of this matrix are zeros and its diagonal terms may be given as

$$\mathrm{diag}([\Psi^*(d_i)]) = \begin{bmatrix} \dfrac{1}{(1-d_1)} \\ \dfrac{1}{(1-d_2)} \\ \dfrac{1}{(1-d_3)} \\ \sqrt{0.5\left[\dfrac{1}{(1-d_1)^2}+\dfrac{1}{(1-d_2)^2}\right]} \\ \sqrt{0.5\left[\dfrac{1}{(1-d_1)^2}+\dfrac{1}{(1-d_3)^2}\right]} \\ \sqrt{0.5\left[\dfrac{1}{(1-d_2)^2}+\dfrac{1}{(1-d_3)^2}\right]} \end{bmatrix} \tag{6}$$

To establish the constitutive relationship pertinent to the anisotropic damage model, the complementary elastic energy of the damaged material is assumed to be equal to the one of the undamaged equivalent material, except that the stresses are replaced by the effective stresses in the energy formulation (Valliappan *et al.* 1999). Equating two energies leads,

$$[\tilde{D}^*] = [\Psi^*]^{-1}[\tilde{D}][\Psi^*]^{-T} \tag{7}$$

where $[\tilde{D}]$ and $[\tilde{D}^*]$ are the material constitutive matrices for undamaged and damaged anisotropic materials, respectively. In the case of 3-D problem, Eq. (7) yields the following relation for $[\tilde{D}^*]$ matrix (Valliappan *et al.* 1999):

$$[\tilde{D}^*] = \begin{bmatrix} d_{11}^* & d_{12}^* & d_{13}^* & 0 & 0 & 0 \\ d_{21}^* & d_{22}^* & d_{23}^* & 0 & 0 & 0 \\ d_{31}^* & d_{32}^* & d_{33}^* & 0 & 0 & 0 \\ 0 & 0 & 0 & G_{12}^* & 0 & 0 \\ 0 & 0 & 0 & 0 & G_{31}^* & 0 \\ 0 & 0 & 0 & 0 & 0 & G_{23}^* \end{bmatrix} \tag{8}$$

in which

$$d_{ii}^* = \frac{E_i^*(1-\nu_{jk}^*\nu_{kj}^*)}{\Delta},\ (j \neq k); \qquad d_{ij}^* = \frac{E_i^*(\nu_{ji}^*+\nu_{ki}^*\nu_{jk}^*)}{\Delta},\ (i \neq j, k \neq i, j \neq k) \tag{8a}$$

$$\Delta = 1 - \nu_{12}^*\nu_{21}^* - \nu_{23}^*\nu_{32}^* - \nu_{13}^*\nu_{31}^* - 2\nu_{21}^*\nu_{32}^*\nu_{13}^* \tag{8b}$$

$$E_i^* = (1-d_i)^2 E_i, \qquad \nu_{ij}^* = \frac{1-d_i}{1-d_j}\nu_{ij}, \qquad G_{ij}^* = \frac{2(1-d_i)^2(1-d_j)^2}{(1-d_i)^2+(1-d_j)^2}G_{ij} \tag{8c}$$

where E_{ij} G_{ij} ν_{ij} are constants for undamaged material. If $d_i = d$, $E_i = E$ and $\nu_{ij} = \nu$ ($i, j = 1, 2, 3$), the isotropic damage model is obtained. In this case, $[\tilde{D}^*]$ can be expressed as

$$[\tilde{D}^*] = (1-d)^2[\tilde{D}] \tag{9}$$

The local constitutive matrix $[\tilde{D}^*]$ can be transformed to the global coordinate directions by assuming the principal directions of damage coincide with the principal stresses. For this case, the standard transformation procedure can be applied and hence the global constitutive matrix $[D^*]$ may be written as

$$[D^*] = [T_\varepsilon]^T[\tilde{D}^*][T_\varepsilon] \tag{10}$$

where $[T_\varepsilon]$ is the standard strain transformation matrix.

2.1 Damage evolution

In present study, the behavior of dam concrete is given by the anisotropic damage model, and it is assumed that the damage occur due to tensile strain only. Damage initiation is determined by the strain threshold corresponding to the tensile strength. In the numerical modeling of mass concrete, the stress-strain diagram of uniaxial loading is used for the strain softening behavior. A widely used assumption in numerical modeling of mass concrete is to adopt a triangular stress-strain diagram for uniaxial loading. This gives a linear strain softening relationship which can be used only as a very rough approximation. Bi-linear, multi linear or exponential softening curves are more consistent with experimental evidences. Definition of exponential softening curve is simpler than those of bi-linear or multi linear ones. However, numerical problems due to suddenly loss of rigidity do not generally occur in the exponential curve because zero-stress level is attained asymptotically in the exponential softening assumption. Therefore, an exponential curve for strain softening model is preferred in this paper. According to Fig. 1(a), an exponential strain softening model (Lubliner *et al.* 1989) yields

$$\sigma(\varepsilon) = E_o\varepsilon \qquad \varepsilon \le \varepsilon_o \tag{11a}$$

$$\sigma(\varepsilon) = f_t[2e^{-a(\varepsilon-\varepsilon_o)} - e^{-2a(\varepsilon-\varepsilon_o)}] \qquad \varepsilon > \varepsilon_o \tag{11b}$$

where f_t and ε_o are the tensile strength and the corresponding strain threshold, respectively. E_o is the modulus of elasticity and the parameter a is a dimensionless constant which can be determined from the following relation (Lubliner *et al.* 1989)

$$a = \frac{3}{\varepsilon_0\left[\dfrac{2E_oG_f}{l_{ch}f_t^2} - 1\right]} \ge 0.0 \tag{12}$$

where the characteristic length (or the fracture band width) l_{ch} is a geometrical constant which is introduced as a measure of the length of the fracture process zone (FPZ) of the material. A consistent characteristic length reduces the width of fracture process zone and it can be expressed as the ratio between the energy dissipated per unit surface area (fracture energy) and the energy dissipated per unit volume (specific energy) at a point (Oliver 1989, Bazant and Cabot 1989). In

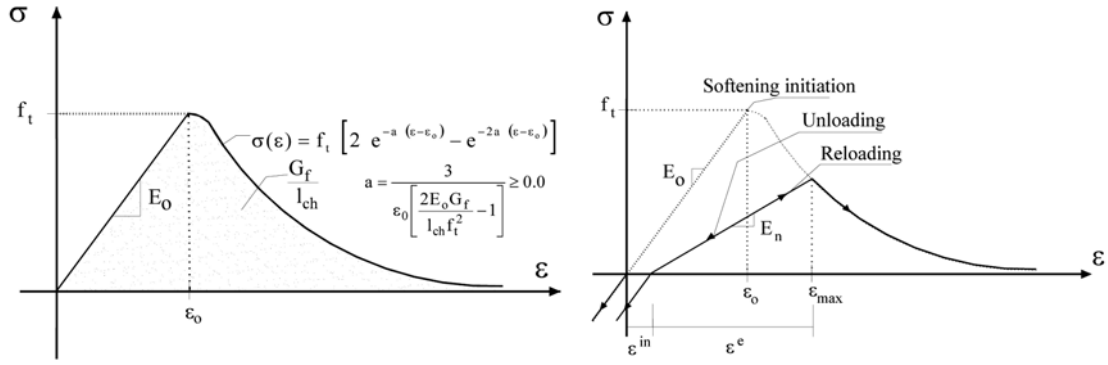

Fig. 1 Constitutive modeling for damage analysis.

this study, this length is calculated from cubic root of the related volume for each integration point of the finite element. G_f is the fracture energy per unit area (Fig. 1a). It can be easily seen from Eq. (12) that the relation of $l_{ch} \leq 2E_oG_f/f_t^2$ has to be provided to develop softening behavior of the material. Based on the hypothesis of strain energy equivalence, the damage parameter for uniaxial loading can be defined as Ghrib and Tinawi (1995)

$$d = 1 - \sqrt{\frac{E^*}{E_o}} \quad \text{or} \quad d = 1 - \sqrt{\left(\frac{\varepsilon_o}{\varepsilon}\right)[2e^{-a(\varepsilon-\varepsilon_o)} - e^{-2a(\varepsilon-\varepsilon_o)}]} \tag{13}$$

It should be noted that there will be three damage variables in the three principal directions for 3-D case.

When the strain is increasing, damage will also increase. During earthquake loading which is cyclic, the strains are reserved and unloading will occur. In the unloading case, permanent strain develops (Fig. 1b). By introducing a fraction λ of the maximum principal strain, $\varepsilon_{\max}$, the total strain is divided into two parts: recoverable elastic ε^e and inelastic strain ε^{in}. Hence, the total strain can be written as follows

$$\varepsilon = \varepsilon^e + \varepsilon^{in} = \varepsilon^e + \lambda\varepsilon_{\max} \tag{14}$$

The value of $\lambda = 0.2$ provides predictions that reflect all essential experimental features (Valliappan *et al.* 1999). When the compressive stress develops, the material gains its original stiffness. Reloading of the crack follows the unloading path until the principal strain is greater than $\varepsilon_{\max}$. When the principal strain is less than ε^{in}, the crack is assumed to be closed. Hence, the unloading-reloading modulus of elasticity becomes (Fig. 1b)

$$E_n = E_o\frac{(1-d)^2}{(1-\lambda)} \tag{15}$$

3. Lagrangian formulation for dynamic interaction of fluid-structure systems

In the Lagrangian approach, displacements are selected as the variables in both fluid and structure

domains. Fluid is assumed to be linearly elastic, inviscid and irrotational. Three-dimensional stress-strain relationships of the fluid undergoing small amplitude motion are given by Calayır (1994)

$$\begin{Bmatrix} P \\ P_x \\ P_y \\ P_z \end{Bmatrix} = \begin{bmatrix} \beta & 0 & 0 & 0 \\ 0 & \alpha_x & 0 & 0 \\ 0 & 0 & \alpha_y & 0 \\ 0 & 0 & 0 & \alpha_z \end{bmatrix} \begin{Bmatrix} \varepsilon_v \\ W_x \\ W_y \\ W_z \end{Bmatrix} \tag{16}$$

where P is the pressure (tension has a positive sign), β is the bulk modulus of fluid and ε_v is the volumetric strain. W_i is rotation parameter about i-axis ($i = x$, y and z). P_i and α_i are the stress and constraint parameter related with W_i, respectively.

Including the small amplitude free-surface waves (sloshing waves) cause pressure at the free-surface of fluid. This pressure can be given by

$$P = -\gamma_f u_{fn} \tag{17}$$

in which γ_f is the weight density of fluid and u_{fn} is the normal component of the free-surface displacement. The free surface stiffness for fluid is obtained from the discrete form of Eq. (17).

Energy dissipation associated with fluid is due to wave radiation in the infinite upstream direction. Sommerfeld radiation condition which is based on one-dimensional wave propagation assumption may be applied to the truncated boundary of reservoir as one way for considering of radiating damping. Hence, analytical explicit representation for pressures along this boundary can be written as El-Aidi and Hall (1989)

$$P = -c\rho_f v_n - c\rho_f v_n^g + P_{st} \tag{18}$$

where P_{st} is the static pressure, c is the fluid pressure wave speed, ρ_f is the fluid mass density, v_n is the normal component of the boundary velocity relative to the free-field velocity and v_n^g is the normal component of the free-field ground velocity.

Finite element equations of motion for the fluid system, using the discrete forms of the equations of (16)-(18) and considering the inertia forces, can be expressed as

$$[M_f]\{a_f\} + [C_f]\{v_f\} + [K_f]\{u_f\} = \{F_f^l\} \tag{19}$$

where $\{a_f\}$,$\{v_f\}$ and $\{u_f\}$ are the relative acceleration, velocity and displacement vectors for the fluid system, respectively $[K_f]$ is the fluid stiffness matrix including the free surface stiffness and $[C_f]$ is the fluid damping matrix due to the radiation damping. $[M_f]$ is the fluid mass matrix, and $\{F_f^l\}$ is the fluid load vector including static loads and earthquake loads due to uniform free-field ground accelerations and earthquake loads associated with the truncated boundary. Reduced integration orders are utilized in the formation of the fluid element matrices.

For obtaining the coupled equations of the fluid-structure system, it is required to determine the interface condition. Because the fluid is assumed to be inviscid, the displacement in normal direction to the interface is only continuous at the interface of the system. This condition can be

imposed by the penalty method (Calayır *et al.* 1996). Using the interface condition, the equations of motion for the coupled system may be given as Karaton (2004), Calayır and Karaton (2005)

$$[M_c]\{a_c\} + [C_c]\{v_c\} + [K_f]\{u_f\} + \{F_s^i\} = \{F_c^l\} \tag{20}$$

where $[M_c]$ and $[C_c]$ represent the mass and damping matrices for the coupled system, respectively. $\{a_c\}$ and $\{v_c\}$ are the relative acceleration and velocity vectors for the same system, respectively. $\{F_s^i\}$ is the restoring force vector for the structure system and $\{F_c^l\}$ is the load vector for the coupled system.

4. Numerical solution of dynamic equilibrium equations of the coupled system

Dynamic equilibrium equations for the fluid-structure systems are given by Eq. (20) in the preceding section. Solution of this equation is carried out in time domain using the improved form of HHT-α integration method presented by Miranda *et al.* (1989). The integration method retains the Newmark difference formulas. However, this method requires to be modified the discrete equations in the time domain, Eq. (20), as follows

$$\begin{aligned}&[M_c]\{a_c\}_{i+1} + (1+\alpha)[C_c]\{v_c\}_{i+1} - \alpha[C_c]\{v_c\}_i + (1+\alpha)[K_f]\{u_f\}_{i+1} \\ &- \alpha[K_f]\{u_f\}_i + (1+\alpha)\{F_s^i\}_{i+1} - \alpha\{F_s^i\}_i = (1+\alpha)\{F_c^l\}_{i+1} - \alpha\{F_c^l\}_i\end{aligned} \tag{21}$$

in which β and γ are Newmark's coefficients and α is a parameter controlling the numerical dissipation. To ensure second-order accuracy and unconditional stability, these parameters should be chosen such that

$$\alpha \in \left[-\frac{1}{3}, 0\right]; \quad \beta = \frac{1}{4}(1-\alpha)^2; \qquad \gamma = \frac{1}{2} - \alpha \tag{22}$$

In this study, α is selected as –0.10.

The predictor-corrector technique is used in conjunction with the Newton-Raphson method to solve the non-linear dynamic equation of fluid-structure interaction problem. The improved form of HHT-α time integration algorithm is given in Miranda *et al.* (1989). If the solution at the time step i is known, the predicted displacement and velocity vectors for the time step $i+1$ can be calculated as

$$\{\tilde{u}_c\}_{i+1} = \{u_c\}_i + \Delta t\{v_c\}_i + \frac{1}{2}\Delta t^2(1-2\beta)\{a_c\}_i \tag{23a}$$

$$\{\tilde{v}_c\}_{i+1} = \{v_c\}_i + \Delta t(1-\gamma)\{a_c\}_i \tag{23b}$$

where subscript c indicates that the quantity is related to the coupled system. If the Newmark difference formulas for displacement and velocity are written in terms of the predicted displacement and velocity vectors given by Eqs. (23a) and (23b), respectively, the following relationships can be obtained:

$$\{u_c\}_{i+1} = \{\tilde{u}_c\}_{i+1} + \beta\Delta t^2\{a_c\}_{i+1} \tag{24a}$$

$$\{v_c\}_{i+1} = \{\tilde{v}_c\}_{i+1} + \Delta t\gamma\{a_c\}_{i+1} \tag{24b}$$

These quantities are substituted into Eq. (21) and then time marching algorithm is applied to Eq. (21) as given in Karaton (2004), Calayır and Karaton (2005).

5. Seismic damage response of arch dam Type 5

In this study, the earthquake damage response of the concrete arch dams was investigated with considering the effects of dam-reservoir interaction. Dam-reservoir interaction was modeled by Lagrangian approach. Fluid is assumed to be linearly elastic, inviscid and irrotational. In the finite element modeling of reservoir, the length of reservoir is considered as two times of its height and Sommerfeld radiating condition was applied to its truncated boundary. The foundation of dam-reservoir system is taken as being rigid. A computer program written in Fortran 95 language by the authors for the linear and non-linear dynamic analyses of dam-reservoir systems was used for the damaged and undamaged solutions (Karaton and Calayır 2004, Calayır and Karaton 2005).

The arch dam Type-5, as suggested in the symposium on arch dams (ICE 1968) in London, was selected for numerical application. The dimensions of this dam are originally defined in dimensionless form. In this study, dimensional form of the dam is obtained such as the height of this dam will be 60 m. The half-finite element mesh of the dam is shown in Fig. 2(a). One nodal point (173) and one element integration point A, for which the time history graphs of the response quantities are plotted, are also marked on this mesh. Eight-noded three-dimensional solid and fluid elements were used in the meshes of the dam and reservoir systems, respectively (Fig. 2b). The number of elements is 196 and 492 for the dam and fluid meshes, respectively. Behavior of undamaged concrete is assumed to be isotropic. The selected material parameters for the concrete are: the elasticity modulus is 31939 MPa, the Poisson's ratio is 0.15, the mass density is 2400 kg/m^3, the tensile strength is 2.519 MPa and the compressive strength is 30 MPa. The fracture energy is computed as 431 N/m by assuming an average aggregate size of 125 mm for mass concrete (CEB-FIB 1991). For including the effect of high strain rate due to dynamic action of earthquake, the tensile strength and the fracture energy are increased by % 20 in the computations. The following

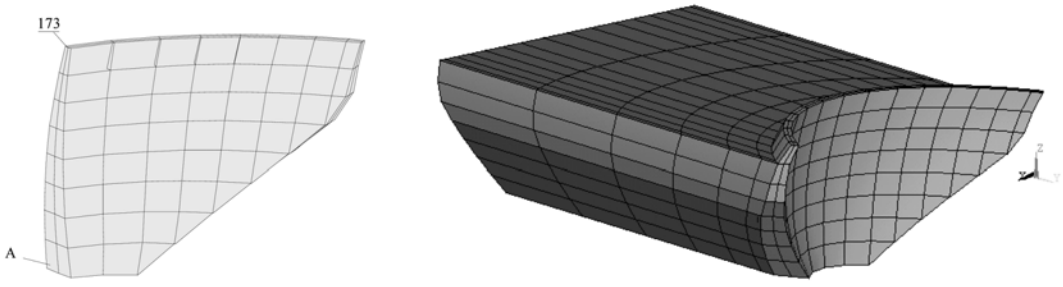

a) The half-finite element mesh of the arch dam b) Finite element model of the dam-reservoir system

Fig. 2 Finite element model used in the analyses

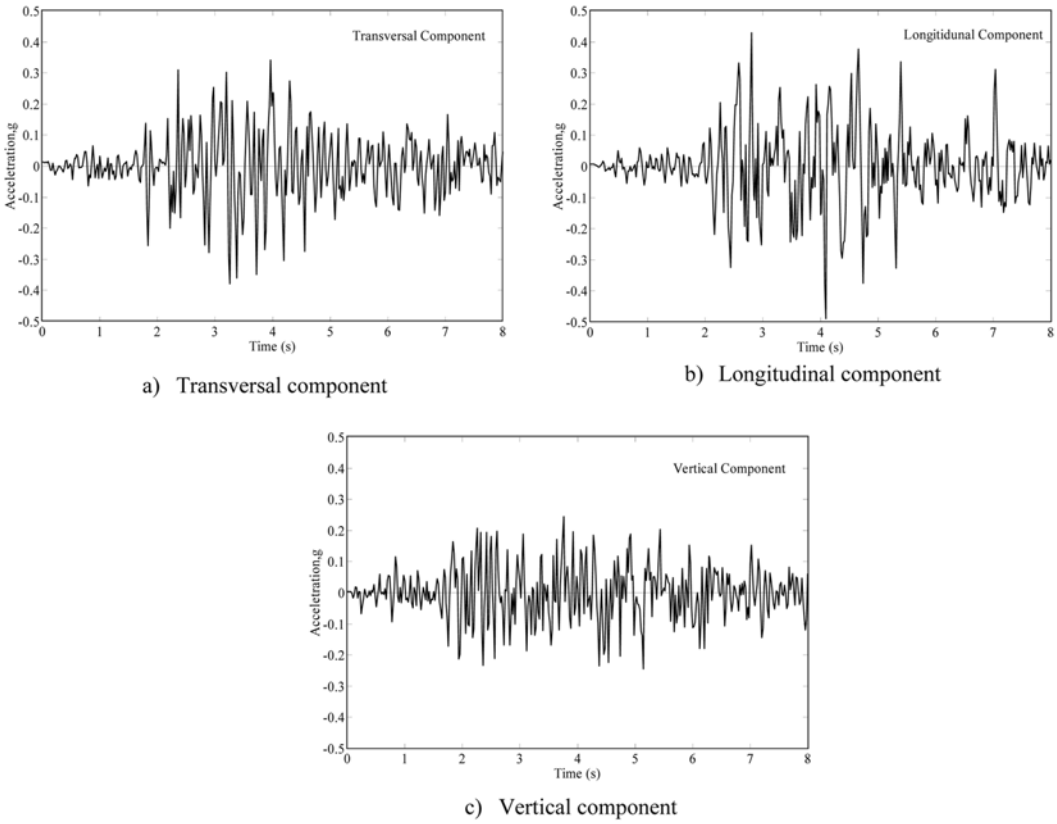

Fig. 3 The Koyna earthquake records

data is considered for the fluid domain: the bulk modulus is 2070 MPa, the mass density is 1000 kg/m^3, and the rotation constraint parameters (three parameters) are chosen as 1000 times of the bulk modulus.

The damping in the dam is assumed as being proportional to the stiffness, and it provides a selected value for critical viscous damping ratio in the fundamental vibration mode for case of no damage in the dam. The damping forces are then computed as proportional to the tangent stiffness matrix for the dam. Integration time step is selected as 0.001 s. For dynamic input, the transversal, longitudinal and vertical acceleration components of 10 December 1967 Koyna earthquake are selected, and it is assumed that they are acting to the dam-reservoir system in the stream, cross-stream and vertical directions, respectively. The records of this ground motion are given in Fig. 3. The static solutions of the dam-reservoir system due to its gravity load were taken as initial conditions in the dynamic analyses of the system.

5.1 Seismic response of the dam with empty reservoir

In this section, the damage response of the arch dam type 5 with no water to the Koyna earthquake is studied. Two solution cases are considered. In the first case, the effect of EASF value on the dam response is investigated for $\xi = 5\%$. For the second one, the effect of damping ratio on

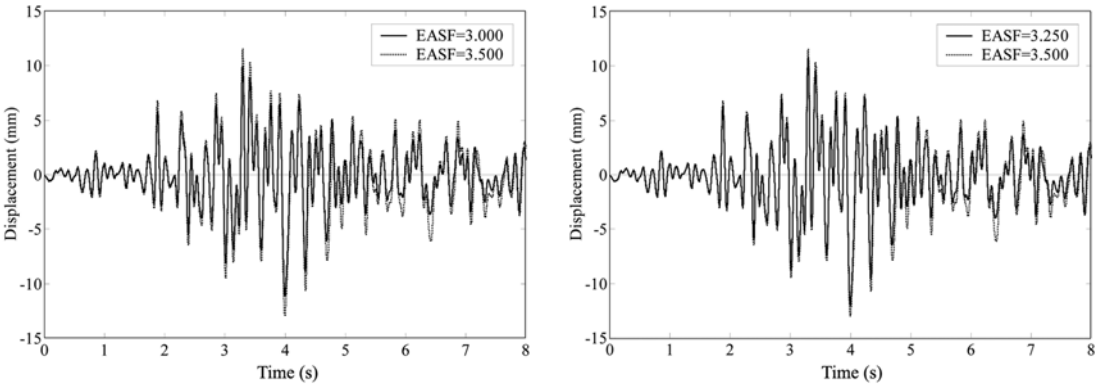

a) Results for EASF values of 3.000 and 3.500 b) Results for EASF values of 3.250 and 3.500

Fig. 4 Radial displacement time history graphs of the dam crest for empty reservoir case

the seismic response of dam is studied for ξ values of 3, 5 and 7%.

There are no hydrostatic and hydrodynamic forces acting on the dam-reservoir interface. To initiate damage in the dam for the first solution case, the EASF values of 1.00, 1.50, 2.00 and 2.50 are insufficient. The ground motion scaled with EASF value of 3.00 induces cracking in the dam. Therefore, the earthquake acceleration amplitudes scaled with EASF values of 3.00, 3.25 and 3.50 are used in the analyses and the obtained results are compared with each other.

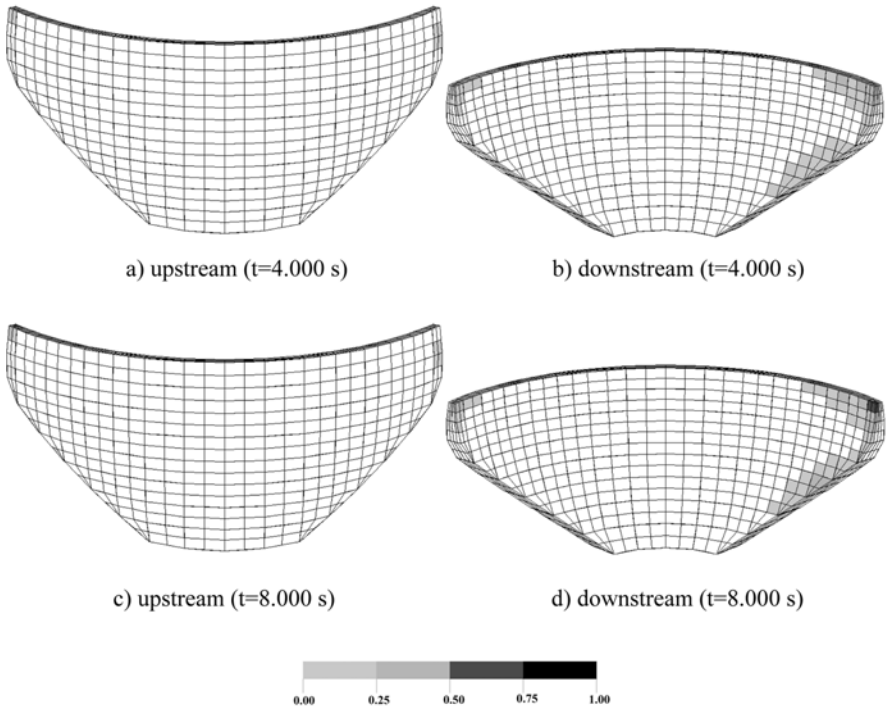

a) upstream (t=4.000 s) b) downstream (t=4.000 s)

c) upstream (t=8.000 s) d) downstream (t=8.000 s)

Fig. 5 Accumulated damage cases in the dam with empty reservoir at 4.00 s and 8.00 s for EASF value of 3.00

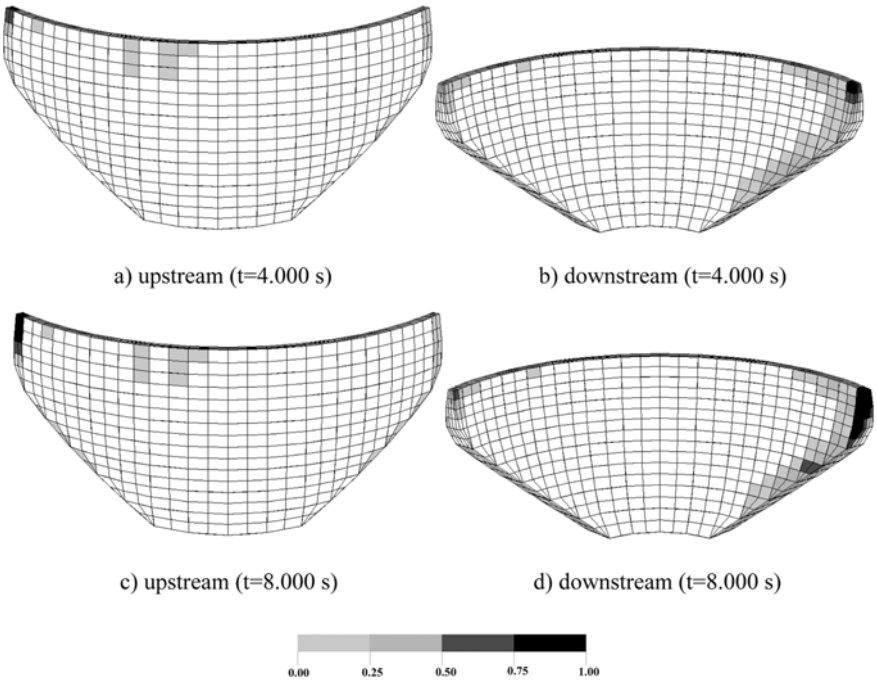

Fig. 6 Accumulated damage cases in the dam with empty reservoir at 4.00 s and 8.00 s for EASF value of 3.25

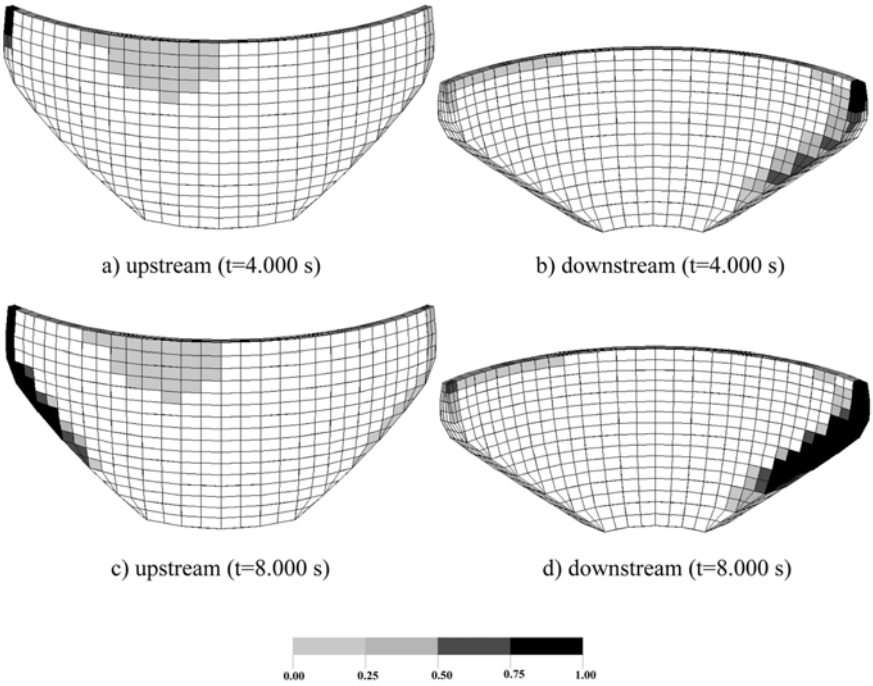

Fig. 7 Accumulated damage cases in the dam with empty reservoir at 4.00 s and 8.00 s for EASF value of 3.50

Fig. 4 shows the time history graphs of the radial displacement of the nodal point 173 located at the dam crest. Positive direction of the radial displacement for this nodal point is in the stream direction. The displacement time histories obtained from the EASF values of 3.00, 3.25 and 3.50 are generally similar in point of frequency contents. However, the displacement amplitudes show an increase as depending on increasing of EASF value. The damage in the dam for the EASF values of 3.00, 3.25 and 3.50 are firstly observed on the middle region of right abutment in the downstream face at 2.449 s, 2.194 and 2.187, respectively. At this location, stresses are concentrated and the tensile stresses reach the largest values.

The accumulated damage cases in the upstream and downstream faces of the dam at 4.00 s and 8.00 s for the EASF values of 3.00, 3.25 and 3.50 are shown in Figs. 5, 6 and 7, respectively. The damage level in a finite element is indicated by shading the element integration point with different tones of black color in the damage plots. Tones of black color vary from slight tone to thick one depending on increasing of damage, for example, thick tone shows much damaged case. Elements that have never damaged (softened) are unmarked in the presentations. Damage level is calculated from the norm of the damage tensor as $d = \sqrt{(d_1^2 + d_2^2 + d_3^2)}$. Significant damage occurs at the middle and upper regions of right abutment in downstream face of the dam, and a relatively narrower area with smaller damage intensity is seen about the upper part of left abutment at the same face. However, damage regions at the upstream face appear as a wide area at left side of the upper arch near to crown cantilever, in addition to the damage regions of both abutments. It is noted that damage regions for all EASF values have generally occurred in the same zones and damage intensities in all damaged regions decrease as depending on decreasing of the EASF value, especially damage region of the upper arch near to crown cantilever in the upstream face does not occur for EASF value of 3.0. Furthermore, damage regions of the dam are unsymmetrical because the cross-stream component of earthquake ground motion is not acted symmetrically to the dam-reservoir system. The softened and complete damaged elements in the damage zones can be closed and reopened at different times depending on the ground motion characteristics. The dam retains its overall stability because the upstream and downstream faces are generally not under tensile stress at the same time.

The global accumulated damage time history graphs obtained for EASF values of 3.00, 3.25 and

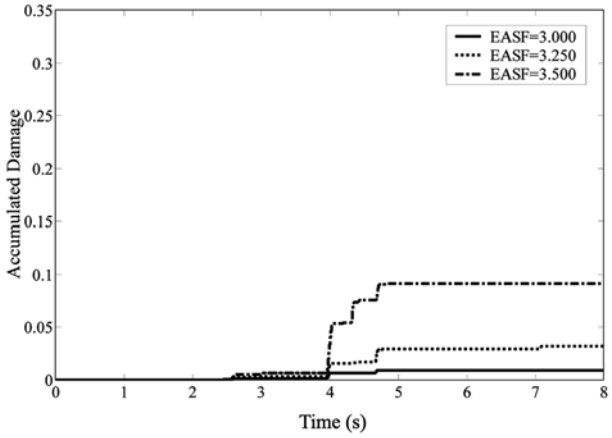

Fig. 8 Time history graphs of the global accumulated damage in the dam with empty reservoir for EASF values of 3.00, 3.25 and 3.50

3.50 are shown in Fig. 8. It can be noted that the important part of damage is usually occurred until 5.0 s. Maximum value of accumulated damage is obtained as 0.94, 3.17 and 9.17% for EASF values of 3.00, 3.25 and 3.50, respectively. It is seen from these results that maximum accumulated

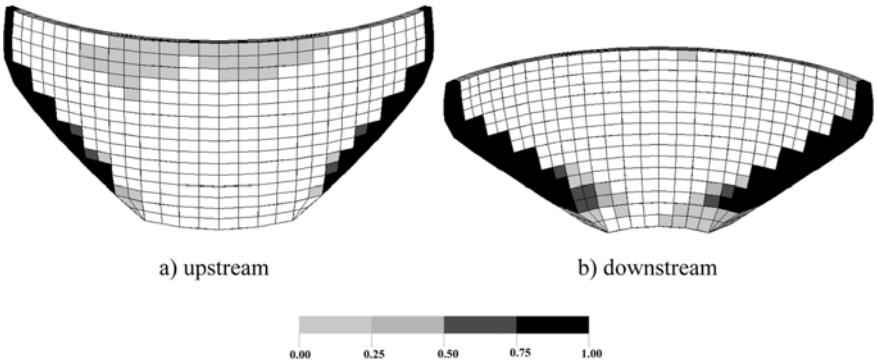

Fig. 9 Accumulated damage cases in the dam with empty reservoir at 4.00 s for damping ratio value of 3%

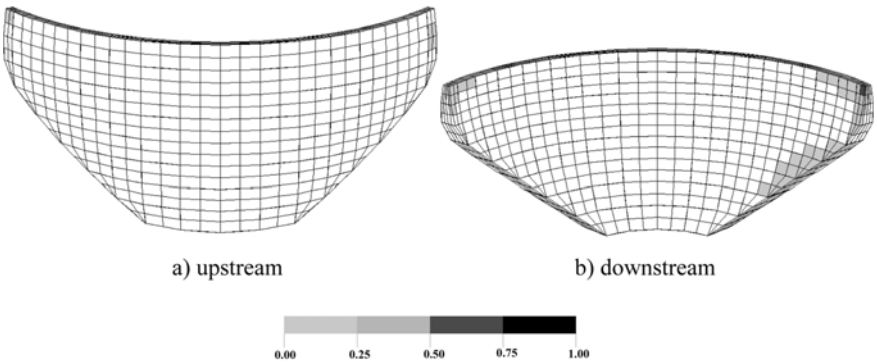

Fig. 10 Accumulated damage cases in the dam with empty reservoir at 4.00 s for damping ratio value of 7%

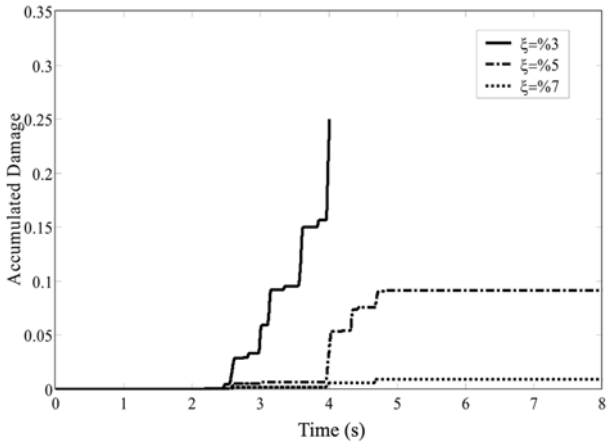

Fig. 11 Time history graphs of the global accumulated damage in the dam with empty reservoir case for damping ratio values of 3, 5 and 7%

damage in the dam increase depending on increasing of the EASF value.

To investigate the effect of damping ratio on the damage response, the EASF value is taken as 3.5 and the results obtained for ξ values of 3, 5 and 7% are compared with each other. The accumulated damage cases on the upstream and downstream faces of the dam for ξ values of 3 and 7% are presented in Figs. 9 and 10, respectively, at 4.0 s. Those of $\xi = 5\%$ were given in Figs. 7(a) and 7(b). Damage regions at both faces of the dam are similar for all damping ratios. The damage intensity and wide of damage regions decrease as depending on increasing of ξ value. Therefore, the damage region of upper arch near to crown cantilever at the upstream face does not occur for ξ value of 7%. The time history graphs of global accumulated damage for three damping ratios are given in Fig. 11. Maximum value of global accumulated damage is 24.98, 9.17 and 0.93 for ξ values of 3, 5 and 7%, respectively. The solution with $\xi = 3\%$ is being unstable at 4.010 s (Fig. 9) because damage occurred in the dam is important level.

5.2 Seismic response of the dam with full reservoir

In this section, the damage response of arch dam type 5 with full reservoir subject to the Koyna earthquake records using EASF value of 1.0 are studied. The selected EASF value is adequate to initiate damage in the dam. It may be noted that for initiating damage in the dam with empty reservoir case, the EASF of 1.00 was insufficient and therefore minimum value of the EASF had been taken as 3.00. Hence, it can be said that the maximum values of seismic response quantities of the full reservoir case are generally larger than those of the empty reservoir case for the same EASF value because of hydrostatic and hydrodynamic forces acting on the dam-reservoir interface.

Fig. 12 shows the time history graphs of the radial displacement of the nodal point 173 located at the dam crest when damage in the dam is allowed and prevented (linear response). Also, Fig. 13 represents those of the maximum and minimum principal stresses occurred in the element integration point A near the base at the upstream face of the dam. The time history graphs of the radial displacement of the dam crest for the damaged and undamaged solutions are similar. However, absolute peak values of the displacements for the undamaged solution generally take lower than those of the damaged case. The maximum principal stresses occurred in the integration point A have

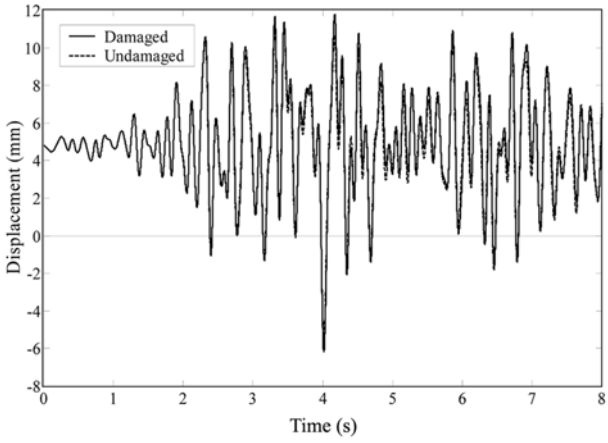

Fig. 12 Radial displacement time history graphs of the dam crest for full reservoir case

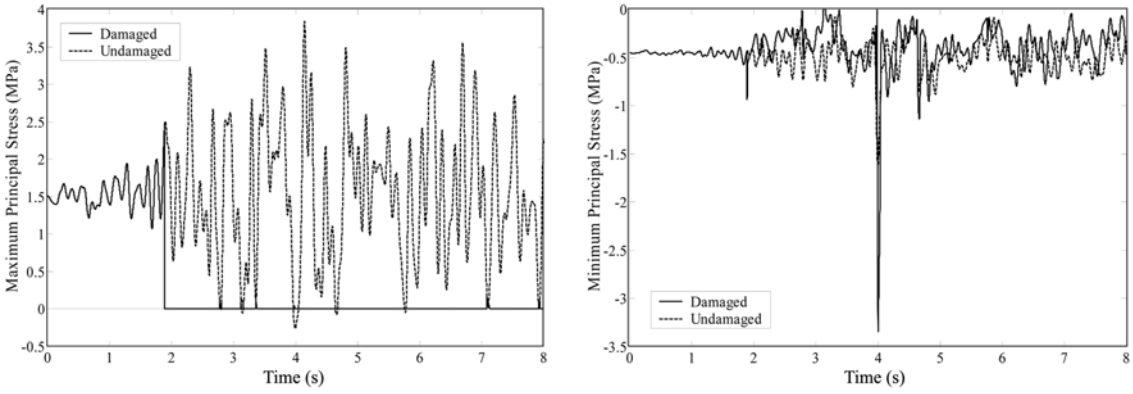

Fig. 13 Time history graphs of maximum and minimum principal stresses at the element integration point of A for full reservoir case (damping ratio value = 5%)

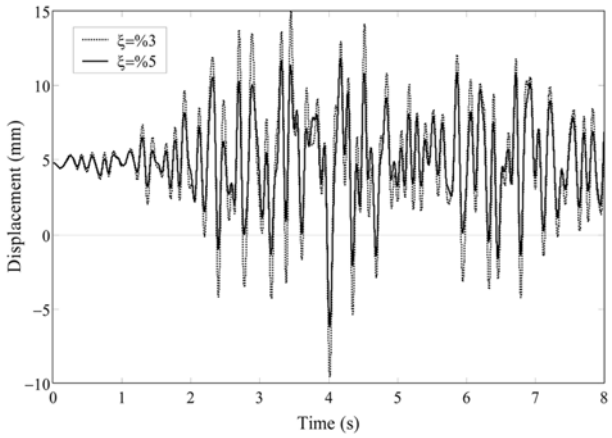

Fig. 14 Radial displacement time history graphs of the dam crest for full reservoir case

showed important differences for two solutions as seen in Fig. 13. While many peak values of the maximum principal stress obtained for the undamaged case take larger than the tensile strength of the concrete, maximum peak value of the maximum principal stress for the damaged case is about the tensile strength. In addition, Fig. 13(a) confirms that tensile strength of the integration point A is completely removed due to importantly increasing of damage intensity at this point after 1.890 s. The minimum principal stresses for two solutions are generally close to each other except the values about 4.000 s. It is seen from these solutions that the maximum compressive stresses obtained for the earthquake records are lower than the compressive strength of the concrete and hence it is not necessary to use two separate damage variables for the tension and compression cases.

To investigate the effect of damping ratio on the damage response of dam-reservoir interaction system, the results obtained for ξ values of 3 and 5% are compared with each other. Solution for ξ value of 7% is not used in the comparison because its damage level is much lower than others. The radial displacement time history graphs of the nodal point 173 are presented in Fig. 14. The displacement time histories obtained for ξ values of 3 and 5% are generally similar in point of

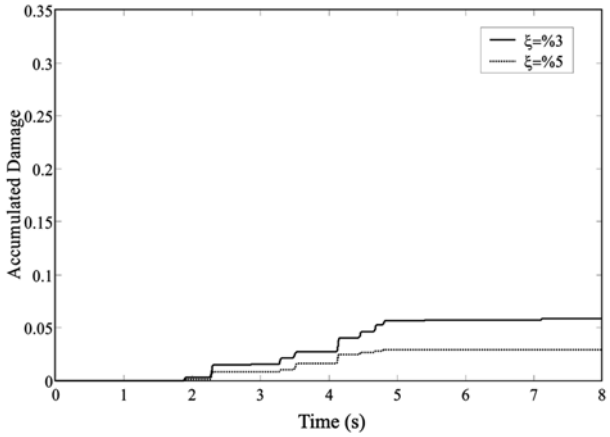

Fig. 15 Time history graphs of the global accumulated damage in the dam with full reservoir case for damping ratio values of 3 and 5%

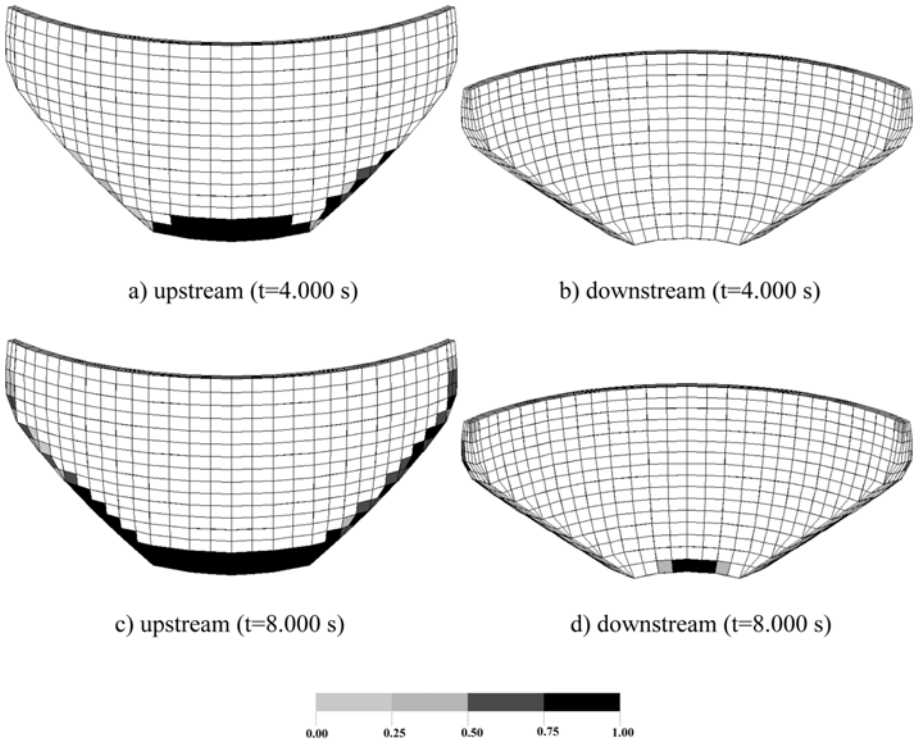

Fig. 16 Accumulated damage cases in the dam with full reservoir at 4.000 s and 8.000 s for damping ratio value of 3%

frequency contents. However, displacement amplitudes show a decrease as depending on increasing of damping ratio value. The global accumulated damage time histories for ξ values of 3 and 5% are given in Fig. 15. Important level of the global accumulated damage develops until the first five seconds as shown in this figure. It is noted that the peak acceleration values of ground motion occur

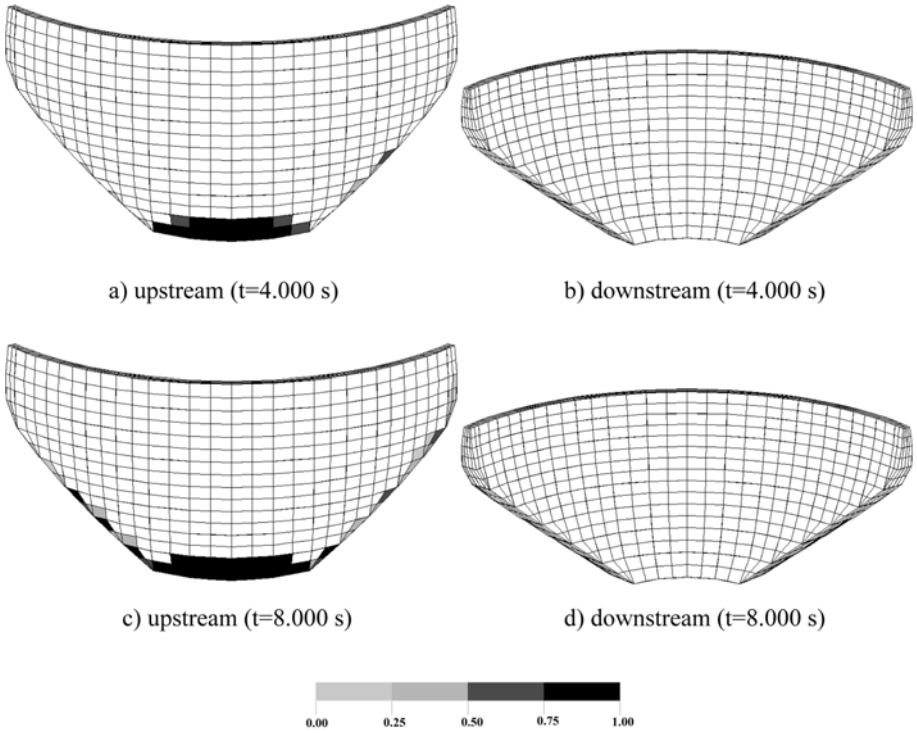

Fig. 17 Accumulated damage cases in the dam with full reservoir at 4.000 s and 8.000 s for damping ratio value of 5%

until this time. The maximum values of global damage for ξ values of 3 and 5% are obtained as 5.909 and 2.959%, respectively. Hence, the maximum value of accumulated damage in the dam decreases as depending on increasing of the damping ratio value.

The accumulated damage cases in the upstream and downstream faces of the dam at 4.00 s and 8.00 s for ξ value of 3% are presented in Fig. 16, and those of 5% are given in Fig. 17. Significant damage occur on the base in upstream face of the dam, and a relatively narrower areas with smaller damage intensity are seen at both abutments of the same face. Any damage region of the upper arch near to crown cantilever does not seen in opposition to the empty reservoir case. However, damage regions at the downstream face are relatively narrower areas than those of the upstream face and the main damage area of downstream face is seen at the dam base. A large stress concentration induces damage propagation at the base of the dam because the foundation is selected as infinitely rigid and hydrostatic and hydrodynamic forces act on the dam. It is noted that damage for ξ values of 3 and 5% are generally occurred in the same regions and damage intensities in all damaged regions decrease as depending on increasing of the damping ratio value.

6. Conclusions

In this study, the earthquake damage response of the concrete arch dams was investigated with considering dam-reservoir interaction. Seismic responses of the concrete arch dam type 5 with

empty/full reservoir cases were obtained by using the 10 December 1967 Koyna earthquake acceleration records.

For empty reservoir case, the effects of the earthquake acceleration scale factor (EASF) and the damping ratio on the dam seismic response were investigated, separately. Damage regions occur about the upper part of left abutment and at the middle and upper regions of right abutment in downstream face of the dam. Damage regions in the upstream face appear as a wide area at left side of the upper arch near to crown cantilever, in addition to damage zones of both abutments. It is noted that damage regions for all EASF values have generally occurred in same zones and damage intensities in all damaged regions decrease as depending on decreasing of the EASF value. Also, damage regions at both faces of the dam are similar for all damping ratios. The damage intensity and wide of damage regions decrease as depending on increasing of the damping ratio value.

In the solutions of the full reservoir case, the EASF value is taken as 1.00. Damaged and undamaged seismic responses of the dam were obtained and results were compared each other. Also, the effect of the damping ratio on damage response of the dam was discussed for full reservoir case. Significant damage occur on the base in the upstream face of the dam, and a relatively narrower areas with smaller damage intensity are seen at both abutments of the same face. Damage at the downstream face was concentrated at the base. Damage regions of this face have narrower areas than those of the upstream face. A large stress concentration induces damage propagation at the base of the dam because the foundation is selected as infinitely rigid and hydrostatic and hydrodynamic forces act on the dam. Damage intensities decrease in all damaged regions as depending on increasing of the damping ratio value.

References

Batta, V. and Pekau, O.A. (1996), "Application of boundary element analysis for multiple seismic cracking in concrete gravity dams", *Earthq. Eng. Struct. Dyn.*, **25**, 15-30.

Bazant, Z.P. and Pijaudier-Cabot, G. (1989), "Measurement of characteristic length of nonlocal continuum", *J. Eng. Mech.*, ASCE, **115**(4), 755-767.

Calayır, Y. (1994), "Dynamic analysis of concrete gravity dams using the Eulerian and the Lagrangian approaches", PhD Thesis, Karadeniz Technical University, Civil Eng. Dept., Trabzon, Turkey. (In Turkish)

Calayır, Y., Dumanoğlu, A.A. and Bayraktar, A. (1996), "Earthquake analysis of gravity dam-reservoir systems using the eularian and lagrangian approaches", *Comput. Struct.*, **59**(5), 877-890.

Calayır, Y. and Karaton, M. (2005), "A continuum damage concrete model for earthquake analysis of concrete gravity dam-reservoir systems", *Int. J. for Soil Dynamics and Earthquake Engineering*, **25**, 857-869.

Comité Euro-International du Béton (1991), *CEB-FIP Model Code 1990*, Thomas Telford, London.

El-Aidi, B. and Hall, J.F. (1989), "Non-linear earthquake response of concrete gravity dams Part 1: Modelling", *Earthq. Eng. Struct. Dyn.*, **18** (6), 837-851.

Ghrib, F. and Tinawi, R. (1995), "An application of damage mechanics for seismic analysis of concrete gravity dams", *Earthq. Eng. Struct. Dyn.*, **24**, 157-173.

ICE (1968), "Arch dams: A review of British research and development", *Proc. of the Symposium Held at the Institution of Civil Engineers*, London, England.

Karaton, M. and Calayır, Y. (2004), "A continuum damage concrete model for earthquake analysis of arch dams", *6th Int. Congress on Advances in Civil Engineering, ACE2004*, Bogazici University, Istanbul, Turkey, October.

Karaton, M. (2004), "Dynamic damage analysis of arch dams including fluid-structure interaction", PhD Thesis, Firat University, Civil Eng. Dept., Elazig, Turkey. (In Turkish)

Lee, J. and Fenves, G.L. (1998), "A plastic-damage concrete model for earthquake analysis of dams", *Earthq.*

Eng. Struct. Dyn., **27**, 937-956.
Lubliner, J., Oliver, J., Oller, S. and Onate, E. (1989), "A plastic damage model for concrete", *Int. J. Solids Struct.*, **25**, 299-326.
Mazars, J. and Pijaudier-Cabot, G. (1989), "Continuum damage theory-application to concrete", *J. Eng. Mech.*, ASCE, **115**, 345-365.
Miranda, I., Ferencz, R.M. and Hughes, T.J.R. (1989), "An improved implicit-explicit time integration method for structural dynamics", *Earthq. Eng. Struct. Dyn.*, **18**, 643-653.
NCR. (1990), *Earthquake Engineering of Concrete Dams-Design, Performance, and Research Needs*, National Academy Press, Washington, DC.
Oliver, J. (1989), "A consistent characteristic length for smeared cracking models", *Int. J. Numer. Meth. Eng.*, **28**, 461-474.
Valliappan, S., Yazdchi, M. and Khalili, N. (1999), "Seismic analysis of arch dams - A continuum damage mechanics approach", *Int. J. Numer. Meth. Eng.*, **45**, 1695-1724.